The Electronic Structure of the Cys-Tyr• Free Radical in Galactose Oxidase Determined by EPR Spectroscopy†

Yuk-Ki Lee, Mei M. Whittaker, and James W. Whittaker*

Department of Environmental and Biomolecular Systems, OGI School of Science and Engineering, Oregon Health and Science University, 20000 Northwest Walker Road, Beaverton, Oregon 97006-8921

Received February 21, 2008; Revised Manuscript Received April 25, 2008

ABSTRACT: Galactose oxidase is a metalloenzyme containing a novel metalloradical complex in its active site, comprised of a mononuclear copper ion associated with a protein free radical. The free radical has been shown to be localized on an intrinsic redox cofactor, 3′-(*S*-cysteinyl)tyrosine (Cys-Tyr), formed by a posttranslational covalent coupling of tyrosine and cysteine side chains in a self-processing reaction. The role of the thioether linkage in the function of the Cys-Tyr cofactor is unresolved, and some computational studies have suggested that the thioether substituent has a negligible effect on the properties of the tyrosyl free radical. In order to address this question experimentally, we have incorporated site-selectively labeled tyrosine (^{2}H, ^{13}C, ^{17}O) into galactose oxidase using an engineered tyrosine auxotroph strain of *Pichia pastoris*. ^{33}S was also incorporated into the protein. EPR spectra for the Cys-Tyr• free radical in each of these isotopic variants were analyzed to extract nuclear hyperfine parameters for comparison with theoretical predictions, and the unpaired spin distribution in the free radical was reconstructed from the hyperfine data. These labeling studies allow the first comprehensive experimental evaluation of the effect of the thioether linkage on the properties of Cys-Tyr• and indicate that previous calculations significantly underestimated the contribution of this feature to the electronic ground state of the free radical.

Free radical mechanisms have emerged as a fundamental feature in enzymology (*1*), where the electronic structure associated with open-valence-shell free radical species can contribute novel, low-barrier pathways in catalysis. Important examples of free radical enzymes have been identified in many fundamental biological processes, including DNA biosynthesis (ribonucleotide reductase, RNR) (*2*), photosynthesis (oxygen-evolving complex, OEC) (*3*), and a wide range of reactions catalyzed by *S*-adenosylmethionine-dependent enzymes (adenosylcobalamin and SAM radical pathways) (*4*), among others.

Galactose oxidase (GAOX)[1] (*5, 6*) is a free radical enzyme in a class of its own. GAOX stabilizes an antiferromagnetically coupled, EPR-silent free radical−copper complex in the active site that performs the two-electron chemistry of alcohol oxidation and dioxygen reduction (eq 1):

$$RCH_2OH + O_2 \rightarrow RCHO + H_2O_2 \qquad (1)$$

A distinctive free radical EPR signal is produced when the metal-free apoenzyme is treated with mild oxidant, showing that the protein itself is redox-active. Spectroscopic and isotopic labeling studies have identified this free radical as being derived from a tyrosine residue (*7*). Subsequently,

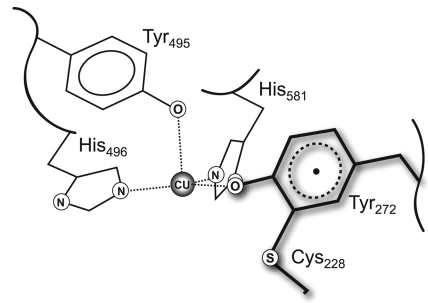

FIGURE 1: Active site of galactose oxidase. The catalytic Cu metal ion and directly coordinated protein side chains are indicated, and the Cys-Tyr cofactor is highlighted. Based on PDB ID 1gog.

X-ray crystallography has revealed a novel thioether covalent cross-link between one of the copper ligands (Tyr272) and a cysteine side chain (Cys228) (Figure 1), providing a likely suspect for the radical-forming site (*8*). This assignment has been confirmed by further spectroscopic analysis and comparison of the free radical formed in the protein with model compounds [e.g., (2-methylthio)cresyl phenoxyl (MTC•)] (*6, 9–11*).

The Tyr272-Cys228 active site cross-link is an intrinsic feature of the galactose oxidase structure, forming a new amino acid, 3′-(*S*-cysteinyl)tyrosine (Cys-Tyr), that serves as an essential cofactor in enzyme function. The Cys-Tyr cofactor has been shown to form spontaneously from a precursor protein lacking the cross-link (*12*) on exposure to Cu(I) and air (*13*), illustrating the ability of a protein to acquire new functionality through posttranslational covalent modification of amino acid side chains. This posttranslational

† This work was supported by National Institutes of Health Grant GM46749 (to J.W.W.).

* To whom correspondence should be addressed. Tel: 503-748-1065. Fax: 503-748-1464. E-mail: jim@ebs.ogi.edu.

[1] Abbreviations: GAOX, galactose oxidase; hf, hyperfine; SOMO, spin occupied molecular orbital; Cys-Tyr, 3′-(*S*-cysteinyl)tyrosine; MTC, (2-methylthio)cresol.

10.1021/bi800305d CCC: $40.75
Published on Web 05/31/2008

modification may, in fact, turn out to be quite widespread in nature, since the Cys-Tyr cofactor has been demonstrated in both eukaryotic (*14*) and prokaryotic (*15*) homologues of galactose oxidase, and a Cys-Tyr cross-link has recently been identified in the structures of both mammalian cysteine dioxygenase (*16, 17*) and a prokaryotic sulfite reductase (*18*), although its function in those enzymes is presently unknown.

The role of the thioether cross-link in the function of the Cys-Tyr cofactor is still unresolved. While the (Cys-Tyr/Cys-Tyr$^{\bullet}$) redox potential is stabilized approximately 200 mV relative to a simple (Tyr/Tyr$^{\bullet}$) phenoxyl (*19*), the extent to which the sulfur side chain participates in the redox chemistry has not been determined, and the possibility of a purely structural role for the cross-link has been raised (*20*). Computational studies have attemped to address this question by investigating the nature of the electronic ground state for the Cys-Tyr cofactor in its oxidized (free radical) form (*20–23*), allowing comparison with the extensive work that has been done to characterize the tyrosyl free radicals in ribonucleotide reductase and photosystem II (*24–26*). These calculations all fundamentally agree on an essentially odd-alternant unpaired electron distribution for the Cys-Tyr$^{\bullet}$ free radical but differ quantitatively in the extent of sulfur contribution to the molecular orbital containing the unpaired electron (SOMO), with predictions ranging from 9% to 28%.

In order to address this question experimentally, we have undertaken the first comprehensive investigation of the electronic structure of the Cys-Tyr$^{\bullet}$ free radical in GAOX using electron paramagnetic resonance (EPR) spectroscopy to resolve electron-nuclear hyperfine (hf) interactions as a direct probe of the unpaired electron distribution. A systematic analysis of the ^{1}H, ^{13}C, ^{17}O, and ^{33}S EPR hyperfine interactions detected in EPR spectra for a series of selectively labeled isotope derivatives of recombinant GAOX (*27*), in which site-selectively labeled tyrosine was incorporated using a *Pichia pastoris* TYR1 auxotrophic expression host (*28*), has yielded a complete set of nuclear hyperfine parameters. The hyperfine coupling constants extracted by simulation of the EPR spectra were then used to map out the unpaired electron spin density distribution on the Cys-Tyr cofactor, experimentally defining the electronic structure of the free radical site of galactose oxidase.

EXPERIMENTAL PROCEDURES

Reagents. L-Tyrosine was purchased from Sigma (St. Louis, MO). [3′,5′-$^{2}H_2$]-L-Tyrosine (98 atom % D) was purchased from Cambridge Isotope Laboratories (Andover, MA). [$^{2}H_7$]-DL-tyrosine (99.2 atom % D) and [2,2′,6′-$^{2}H_3$]-DL-tyrosine (98.1 atom % D) were obtained from CDN Isotopes (Pointe-Claire, Québec). [2,2′,3′,5′,6′-$^{2}H_5$]-DL-Tyrosine (97 atom % D) was synthesized essentially as described by published procedures (*29*), except that the reaction was performed under argon at 145−150 °C for 2 days, and at the end the reaction mixture was adjusted to pH 4.5 with concentrated NH_4OH in an ice bath. This exchange reaction was repeated (2×) to achieve the highest isotopic substitution. ^{13}C-Labeled L-tyrosine derivatives were purchased from Cambridge Isotope Laboratories: [4′-^{13}C]-L-tyrosine (95.9 atom % ^{13}C), [3′,5′-$^{13}C_2$]-L-tyrosine (99.1 atom % ^{13}C), and [ring-$^{13}C_6$]-L-tyrosine (99 atom % ^{13}C). ^{17}O-Labeled tyrosine ([4′-^{17}O]-L-tyrosine, 50 atom % ^{17}O) was obtained from Isotec (Miamisburg, OH). ^{33}S metal (99.92 atom % ^{33}S) was obtained from Cambridge Isotope Laboratories. ^{33}S was oxidized to sulfate by treatment with bromine in aqua regia (*30*). Briefly, 50 mg of elemental sulfur was added to 1 mL of aqua regia containing 200 μL of bromine, and the sulfur particles were dispersed in an ultrasonic bath. After all of the sulfur had dissolved and oxidized, the excess bromine was eliminated in a stream of argon. The resulting acid solution was neutralized with sodium hydroxide and heated to boiling. After cooling, the volume was made up to 5 mL with deionized water, and the solution was filter sterilized (0.2 μm filter).

Diphenylpicrylhydrazyl (DPPH) (Eastman Kodak, Rochester, NY) was recystallized from benzene for field/frequency calibration of EPR spectra ($g_{DPPH} = 2.0036 \pm 0.0003$ (*31*)). Recrystallized DPPH was sealed in 0.040 in. i.d. Tygon microbore tubing with Instant Krazy Glue.

Biological Materials. Previously described *P. pastoris* X33::PICZαGAOX (*27*) and *P. pastoris* TYR1::PICZαGAOX (*28*) galactose oxidase expression strains containing a methanol-induced expression cassette integrated into the genome were maintained and cultivated on yeast−peptone−dextrose (YPD) (*32*) or standard defined (SD) minimal medium containing 0.17% YNB (yeast nitrogen base without amino acids and ammonium sulfate; Difco) supplemented with 0.5% ammonium sulfate, 2 mL of 0.02% biotin, 1 mL of PTM4 trace metal solution, 60 mM potassium phosphate buffer, and tyrosine (100−150 mg/L).

Protein Expression and Purification. Isotopically labeled GAOX was produced by a *P. pastoris* TYR1 heterologous expression host (*28*) in chemically defined expression medium with labeled tyrosine or [^{33}S]sulfate. For tyrosine labeling, 20 mL of phosphate-buffered SD with 2% glucose supplemented with 150 mg/L unlabeled tyrosines was inoculated in a 125 mL baffled flask using freshly grown expression strain culture and grown at 30 °C with shaking. The culture was centrifuged in sterile Oak Ridge tubes, and the cells were resuspended in 1 L of 2× phosphate-buffered SD with 2% glucose and labeled amino acid in a 2 L baffled flask. The culture was allowed to grow at 30 °C with shaking to stationary phase. Cells were centrifuged and resuspended in 200 mL of 2× phosphate-buffered expression medium (SD containing 20 μM $CuSO_4$ and labeled amino acid) in a 2 L baffled flask. Galactose oxidase expression was induced with 0.5% methanol added daily for 4 days at 30 °C with shaking (*27*). For sulfur labeling, an aliquot of 10 mg/mL ^{33}S stock solution (prepared as described above) was added to sulfate-free minimal growth medium (1 mL/L) for expression of ^{33}S-labeled GAOX. *Pichia* cell biomass was removed from the fermentation culture, and GAOX was purified according to the published procedures (*33*). Mass spectroscopic analyses of tryptic peptides of the ^{33}S-labeled GAOX were performed on the QSTAR XL or on the QTRAP4000, and the results were analyzed with the program IsoFit.[2] Briefly, the extent of ^{33}S incorporation was measured by calculating the expected isotopic distributions for each of the peptides, one containing only natural abundance isotopes and the others containing up to 100% ^{33}S. The observed isotopic peaks in the mass spectrum were then modeled (using maximum likelihood methods) to estimate

[2] L. David and L. Rustvold, to be published.

the percentage of sulfur sites with ^{33}S incorporation, varying the proportions of the calculated distributions. The fitting also included distributions resulting from partial deamidation, which introduces a unit mass increase ($\Delta m/z = 1$ amu) in peptides containing asparagine and glutamine. Finally, peak shape parameters were included to fine-tune the fit to the data. This analysis indicated a labeling efficiency of 98 ± 2 atom % for ^{33}S-labeled galactose oxidase.

Preparation of Cys-Tyr• Free Radical. Metal-free apoGAOX was prepared by a modified chelation procedure (*7*). Briefly, a concentrated diethyl dithiocarbamate solution (200 mM) was added to 0.5 mM GAOX solution with an 8-fold excess. The yellow mixture was centrifuged at high speed, leaving a colorless supernatant from which unreacted reagent was removed by gel filtration (Bio-Gel P-30). Oxidized apoGAOX was prepared by adding 50 mM $K_3Fe(CN)_6$ to the metal-free enzyme and desalting.

Spectroscopic Measurements. X-band (9.2−9.9 GHz) EPR spectra were recorded using a Bruker ELEXSYS E500 spectrometer equipped with a Bruker ER049X SuperX X-Band microwave bridge, Bruker ER4122SHQE superhigh Q high-sensitivity cavity, and a E27H lock-in detector. Temperature control was provided by a continuous nitrogen flow cryostat system, with temperature monitoring by a Bruker W1100321 thermocouple probe. The EPR spectra were displayed and analyzed using the Bruker XeprView interface. The EPR spectrometer and cryostat system were stabilized for 2−3 h before the data were collected. First harmonic X-band EPR spectra of the ^{2}H-labeled, ^{13}C-labeled, ^{33}S-labeled, and ^{17}O-labeled samples were collected at both low [50 μW (36 dB)] and high [20 mW (10 dB)] microwave power. In all of the experiments, first harmonic spectra of free radical DPPH were collected for field/frequency calibration at 50 μW (36 dB) and 20 mW (10 dB) immediately before and after collecting the spectra of the protein samples. Under these conditions, the relaxation-narrowed powder spectrum of the solid DPPH sample dominated the spectrum, even though it rested on top of the frozen protein sample. A duplicate set of EPR spectra was collected for each sample to confirm the accuracy of the data.

The concentration of the free radical in protein samples was calculated by comparing the double-integrated EPR intensity with the corresponding value obtained for a 1 mM $Cu(ClO_4)_2$ spin standard in 2 M $NaClO_4$ based on standard methods. Baseline and field (ΔH_{corr}) corrections were applied to the experimental spectra in the Bruker XeprView interface. The field correction was calculated by comparing the known *g*-value of DPPH with the observed *g*-value (eq 2):

$$\Delta H_{corr} = h/\beta(\nu/g_{DPPH}) - H_{obs} = H' - H_{obs} \quad (2)$$

where h is Planck's constant, β is the Bohr magneton, ν is the frequency (in megahertz), g_{DPPH} is the literature *g*-value of DPPH ($g_{DPPH} = 2.0036$) (*31*), H_{obs} is the observed crossing point (in gauss), and H' is the predicted crossing point calculated using the literature *g*-value of DPPH. The ΔH_{corr} correction was typically on the order of 1 G.

EPR Power Saturation Analysis. Power saturation measurements of unlabeled Cys-Tyr• oxidized apoGAOX were performed at 100 K with 1 G modulation amplitude. The X-band (9.394 GHz) spectra were collected over a microwave power range (0.2 μW−200 mW, 60 dB−0 dB) and calibrated with DPPH. Baseline corrected spectra were imported into Specfit 3.0 global fitting data analysis software (Spectrum Software Associates, Marlborough, MA) and analyzed using the model-free evolving factor analysis (EFA) routine. This method factor-analyzes the spectra and resolves component spectra (basis vectors) from the entire data set. The two spectral components extracted by EFA together with the spectroscopic intensities recorded during the power saturation experiment were imported into the graphing program Kaleidagraph (Synergy Software, Reading, PA) for further analysis. The power dependence of each of the two components was fit using least-squares methods to an equation of a form (eqs 3 and 4) (*34*):

$$\log(I/\sqrt{P}) = -(b/2)\log(P_{1/2} + P) + (b/2)\log(P_{1/2}) + \log k \quad (3)$$

$$= \log\left(\frac{P_{1/2}k^{2/b}}{P_{1/2} + P}\right)^{b/2} \quad (4)$$

where I is the signal intensity, $P_{1/2}$ is the microwave power required for half-saturation, P is the microwave power, b is the inhomogeneity factor, and k is a proportionality (scaling) factor.

The recorded spectroscopic intensities of the raw data were also fit using least-squares methods. Since the raw data are essentially the sum of the two components, an additional term is required (eq 5):

$$\log(I/\sqrt{P}) = \log\left[\sum_{i=1}^{2}\left(\frac{(P_{1/2})_i k_i^{2/b_i}}{(P_{1/2})_i + P}\right)^{b_i/2}\right] \quad (5)$$

where $(P_{1/2})_i$ are saturation parameters for the low- and high-power components ($i = 1, 2$), respectively. A plot of $\log(I/\sqrt{P})$ vs microwave power was obtained, and the values of $P_{1/2}$, b_i, and k_i were determined by fitting the power dependence of the resolved components.

EPR Simulation Procedures. Spectra were simulated using a continuous wave (CW) EPR computer simulation software suite [XSophe 1.1.4 (*35*)] to extract detailed structural information, including *g*-values and hyperfine coupling constants. For a simple paramagnetic system ($S = {}^1/_2$) with anisotropic *g*-values and hyperfine coupling constants, the spin Hamiltonian ($\mathscr{H}$) takes the form (eq 6):

$$\mathscr{H} = \beta H \cdot \boldsymbol{g} \cdot S + \sum S \cdot \boldsymbol{A} \cdot I \quad (6)$$

where S is the electron spin operator, I is the nuclear spin operator, $\boldsymbol{g}$ is the electronic Zeeman tensor, $\boldsymbol{A}$ is the total hyperfine coupling tensor (with principal components A_{xx}, A_{yy}, and A_{zz}, including both isotropic and dipolar terms), β is the Bohr magneton, and H is the applied magnetic field.

In XSophe, the EPR spectrum is calculated by integrating the magnetic dipole transition moment, convoluted with a line shape function, over spherical angles to simulate the orientation-averaged spectrum of a randomly oriented powder sample (eq 7) (*35*):

$$S(H,\nu_c) = \sum_{i=0}^{N}\sum_{j=i+1}^{N} C\int_{\theta=0}^{\pi}\int_{\phi=0}^{\pi} |\mu_{ij}|^2 f[\nu_c - \nu_o(H),\sigma_\nu]\, d\cos\theta\, d\phi \quad (7)$$

where $S(H,\nu_c)$ denotes the spectral intensity, $|\mu_{ij}|^2$ represents the magnetic dipole intensity for the $i \rightarrow j$ transition evaluated from the spin Hamiltonian (eq 6), ν_c is the microwave

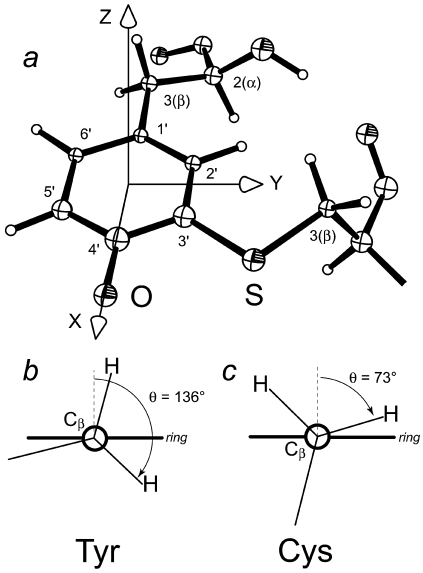

FIGURE 2: Cys-Tyr cofactor structure. (a) Ball-and-stick model of the galactose oxidase Cys-Tyr cofactor rendered using the program Ortep3, with the superimposed coordinate system defining the principal axis directions. The side chain atom numbering scheme is indicated. (Below) Headgroup dihedral for (b) Tyr272 C_β and (c) Cys228 C_β. Based on PDB ID 1goh.

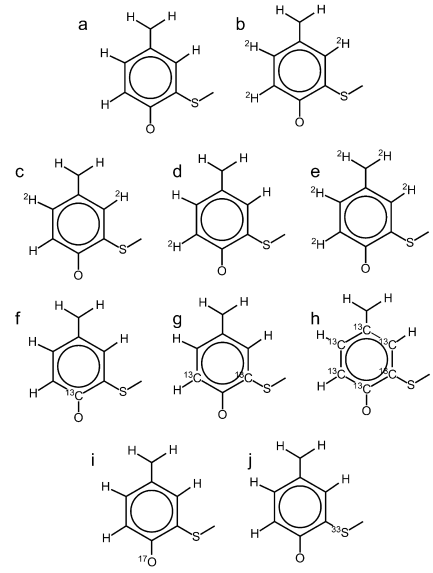

FIGURE 3: Cys-Tyr isotopomers investigated in this study: (a) unlabeled; (b) [2,2′,5′,6′-$^2H_4$]-L-cysteinyltyrosine; (c) [2,2′,6′-$^2H_3$]-L-cysteinyltyrosine; (d) [5′-$^2H_1$]-L-cysteinyltyrosine; (e) [2,3,3,2′,5′,6′-$^2H_6$]-L-cysteinyltyrosine; (f) [4′-^{13}C]-L-cysteinyltyrosine; (g) [3′,5′-$^{13}C_2$]-L-cysteinyltyrosine; (h) [ring-$^{13}C_6$]-L-cysteinyltyrosine; (i) [4′-^{17}O]-L-cysteinyltyrosine; (j) [^{33}S]-L-cysteinyltyrosine.

frequency, $\nu_o(H)$ is the resonant frequency, σ_ν is the line width, $f[\nu_c - \nu_o(H), \sigma_\nu]$ is the line shape function (Gaussian or Lorentzian), θ and φ are the polar and azimuthal angles, respectively, and C is a normalization constant.

The CW powder spectra were calculated in XSophe using full matrix methods for the electronic parameters while the hyperfine terms were treated perturbatively. The composition of the spin system and the isotopic abundance for each paramagnetic nucleus was defined for each free radical protein sample at the start of the calculation. Initial estimates of the spin parameters (g-values, hyperfine coupling constants, and line widths) were entered along with limits (deviations and parameter half-spaces) for optimization. A Hooke and Jeeves optimization method was used, normalizing the calculated spectra to the peak extrema of the experimental data. Ideally, a global fitting procedure would be applied to simultaneously optimize all shared parameters over the entire series of spectra. This is not possible in the current implementation of XSophe, so we adopted an iterative approach, sequentially optimizing parameters over the set of spectra to achieve self-consistency in the parameter set. All spectra were corrected both for field/frequency calibration and to subtract the secondary (high-power) spectral component. Numerical differentiation of the normal EPR spectrum was used to enhance the fine structure, contributing to the quality of the fit. Both normal (absorption derivative) spectra and second derivative transforms were fit by XSophe simulation, with the second derivative EPR absorption spectra being fit by second harmonic simulation in XSophe. All parameters underwent iterative optimization over the entire set of spectra, converging to self-consistent values for each of the parameters. This final, refined set of parameters was used to reproduce the entire set of spectra, including all isotopomers. In order to compensate for residual errors in the experimental data, the parameters were allowed to vary approximately 10% from the optimized value during the final iteration, although the optimized value was fixed during this process. As a result, the minimum relative uncertainties in the parameters may be taken as 10% of the stated value.

Spin Density Analysis. The experimental hyperfine tensors were resolved into isotropic (A_{iso}) and anisotropic (T) parts, and these components were used to solve for the unpaired spin density distribution over the six ring carbon atoms, the phenoxyl oxygen, and the thioether sulfur of the Cys-Tyr$^\bullet$ free radical. The experimental hyperfine tensor components were entered as data in the program Scientist (MicroMath, St. Louis, MO) together with the equations relating each of the hyperfine tensors to components of electronic spin density. Global minimization of the differences between experimental and predicted hyperfine components over the entire set of data (Levenberg−Marquardt algorithm) was used to optimize the spin density distribution. This approach provides an estimate of a consensus unpaired spin distribution that is consistent with the entire experimental data set.

RESULTS AND DISCUSSION

EPR Measurements. Power saturation measurements were performed on oxidized, unlabeled apoGOAX Cys-Tyr$^\bullet$ samples at microwave powers ranging from 0.2 μW to 200 mW (60 dB−0 dB) (Figure 4). The resulting spectra, shown as a 3D stack plot in Figure 4, progressively increase in amplitude with increasing power (at constant gain) to a maximum amplitude near 100 μW, above which the amplitude decreases and the line shape dramatically changes, suggesting the presence of a second paramagnetic species in the sample. In order to investigate this possibility, the entire set of spectral data arising from the power saturation experiment was assembled into a rectangular data array and analyzed using global fitting matrix methods [model-free extended factor analysis (EFA)] to extract component spectra (Figure 5, inset). In addition to resolving basis spectra from the composite data set, the EFA method yielded the power dependence for each of the components. A plot of $\log(I/\sqrt{P})$ vs microwave power for both components and for the

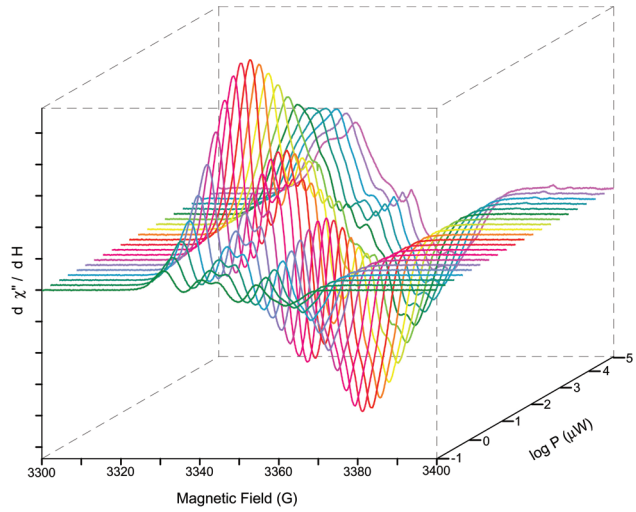

FIGURE 4: Power saturation of oxidized apoGAOX free radical EPR spectra. 3D stack plot for spectra recorded for oxidized apoGAOX (1.3 mM in 25 mM $KHPO_4$ buffer, pH 7) at a microwave power ranging from 0.2 μW to 200 mW. Instrumental parameters: microwave frequency, 9.394 GHz; modulation frequency, 1 G; temperature, 100 K.

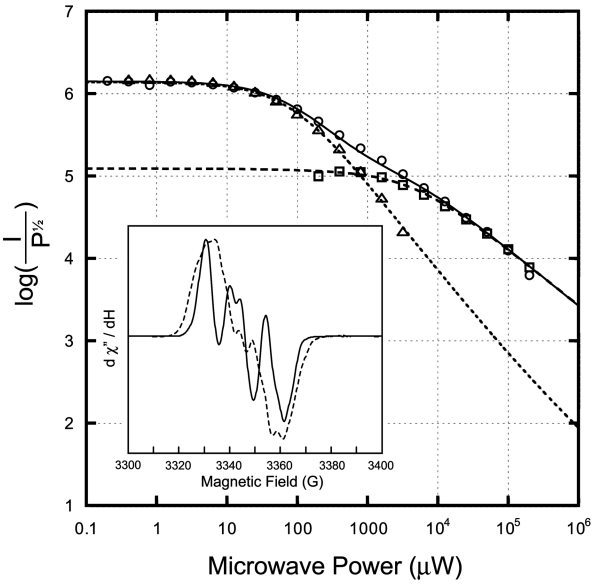

FIGURE 5: Power saturation profile for apoGAOX free radical EPR spectra: total intensity (circles); low-power component (triangles); high-power component (squares). Lines represent least-squares fits to the theoretical power dependence (eqs 4 and 5): (solid line) total; (dotted line) low-power component; (dashed line) high-power component. Inset: Resolved spectral components derived from model-free evolving factor analysis of data: (solid line) low-power component; (dashed line) high-power component.

raw power saturation data is shown in Figure 5. The low- and high-power components match the low-power ($P < 100$ μW) and high-power ($P > 10$ mW) regions of the experimental data, respectively, confirming the presence of two distinct EPR-active components, saturating at different microwave powers, in the sample. When the data for the discrete, resolved components were fit with eq 4, parameters describing the saturation behavior for each component were obtained. The primary free radical, the component which dominates at low power, has a spectrum essentially identical to that previously reported for the Cys-Tyr• free radical in oxidized apoGAOX (*7*). This component saturates relatively easily [$P_{1/2} = 86$ μW (34 dB)] and has an exponential factor (inhomogeneity factor, $b = 2.27$) reflecting an essentially Lorentzian, homogenously broadened line (which would yield $b = 3$). The secondary free radical, which dominates the EPR spectrum at high power, is clearly distinct. This component is more difficult to saturate [$P_{1/2} = 4055$ μW (16 dB)], indicating a more efficient spin−lattice relaxation mechanism, and is associated with an inhomogeneity factor ($b = 1.37$) close to the Gaussian limit (corresponding to $b = 1$). The relative abundance of the two components can be estimated from the spectral amplitudes for each in the low-power limit (Figure 5): the low- and high-power components are found to represent 92% and 8% of the total signal intensity at low power, respectively. Based on spin quantitation, the total concentration of free radicals in the sample (1.3 mM oxidized apoGAOX) is 0.22 mM corresponding to an overall yield of 17%.

The results of the power saturation experiments guided the choice of instrument settings used to acquire spectra for each of these paramagnetic species. For each sample, both low-power [50 μW (36 dB)] and high-power [20 mW (10 dB)] spectra were collected, and following normalization (based on the integrated signal intensity), the appropriate amount of the high-power spectrum was subtracted, yielding the isolated Cys-Tyr• free radical spectrum for detailed analysis.

EPR spectra were measured for both unlabeled apoGAOX Cys-Tyr free radical and nine distinct isotopomers (Figure 3), prepared by selective isotopic labeling. Labeled tyrosine was incorporated into galactose oxidase by an engineered tyrosine auxotroph expression strain (*P. pastoris* TYR1) (*28*). Although the isotopic substitution was selective within each tyrosine side chain, all tyrosines in the protein were equally labeled. The tyrosine supplied in the medium is the sole source of this amino acid in the *P. pastoris* TYR1 expression strain, so the labeling efficiency is determined by the isotopic enrichment of the supplemented amino acid. The isotope derivatives may be divided into four groups: ^{2}H-labeled (Figure 3b−e), ^{13}C-labeled (Figure 3f−h), ^{17}O-labeled (Figure 3i), and ^{33}S-labeled (Figure 3j). Since all of these isotopes possess nonzero nuclear spin (I), their interactions with the unpaired electron of the free radical split the EPR signal, and these electron-nuclear hyperfine splittings reflect the unpaired electron distribution of the free radical (eq 6).

For ^{1}H/^{2}H hyperfine analysis, spectra for samples including only these isotopes were examined (Figure 3a−e). A total of 21 parameters (five ^{1}H/^{2}H hf tensor principal values, three g-values, three line widths) were routinely included in the simulations. ^{2}H hf tensors were scaled from the corresponding ^{1}H hf tensors based on the magnetogyric ratios for ^{1}H and ^{2}H nuclei (γ^1H = 26.7522 × 10^7 rad s^{-1} T^{-1}; γ^2H = 4.1066 × 10^7 rad s^{-1} T^{-1}). The electronic g-values for the Cys-Tyr• free radical were initially optimized by analysis of data for the perdeuterated cofactor (Figure 3e) which exhibits the narrowest EPR spectrum ($\Gamma_{fwhm} = 9$ G) (Figure 6). These values were subsequently fixed for analysis of data for the other isotopomers in order to evaluate the ^{1}H hf tensor components and then iteratively adjusted in a simulation of perdeuterated Cys-Tyr• using the scaled ^{2}H hf tensor components (γ^1H/γ^2H = 6.51). The H_β hf parameters were initially optimized through simulation of the EPR spectrum of the fully ring-deuterated derivative (Figure 3b, Figure 7b) and subsequently refined to self-consistency over the com-

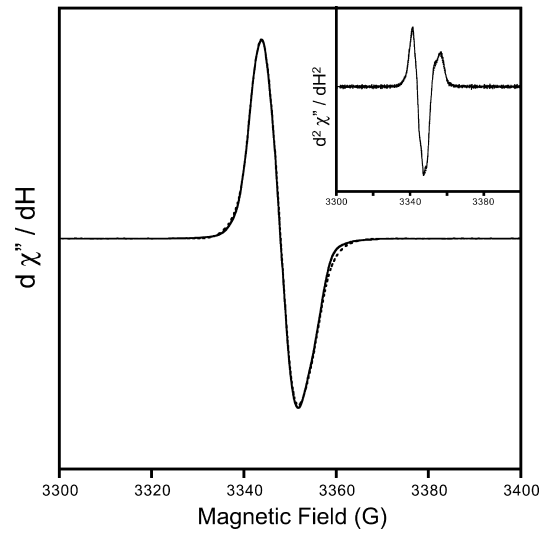

FIGURE 6: EPR spectrum of perdeuterated Cys-Tyr. Oxidized apoGAOX labeled with [$^2H_7$]-DL-tyrosine (0.8 mM protein in 25 mM $KHPO_4$ buffer, pH 7) and oxidized as described in the Experimental Procedures. Inset: Second derivative EPR spectrum. (Dashed line) XSophe simulation as described in the Experimental Procedures using the parameters in Table 1. Instrumental parameters: microwave power, 50 μW; microwave frequency, 9.398 GHz; modulation frequency, 1 G; temperature, 100 K.

plete set of EPR spectra. Ring ^{1}H hf parameters were optimized by iterating between spectra for corresponding labeled and unlabeled samples. Parameters for ring ^{13}C nuclei were similarly obtained. The hf parameters for O and S positions were evaluated using the self-consistent parameters obtained for unlabeled Cys-Tyr$^\bullet$ (g-values, hf tensors, and line widths). The final set of hf parameters (Table 1, columns 3−5) could be used to reproduce the complete set of EPR spectra (Figures 6–9).

Because the labeling of the tyrosine ring is symmetrical, there is an unavoidable ambiguity in assignment of certain positions (2′/6′, 3′/5′) which cannot be resolved directly in these experiments. However, certain structural features of the Cys-Tyr cofactor indirectly aid in these assignments. For example, the lack of a ring H at the 3′ position in the Cys-Tyr cofactor (Figure 2) leaves a unique hydrogen at the 5′ position, allowing the 5′-^{1}H/^{2}H hf parameters to be assigned on the basis of data for [3′,5′-$^2H_2$]tyrosine. This unique feature also helps to resolve the ambiguity in the ^{13}C hf parameters for 3′ and 5′ positions (Figure 3g) since the carbon and hydrogen hf interactions report on the same local electron density and must be correlated. In other cases, remaining ambiguity was addressed by relating to hf parameters at neighboring, well-defined positions (*vide infra*). Similar approaches were used to characterize the minority species that gives rise to the EPR signal detected at high microwave power.

EPR Parameters. g-Values. The self-consistently optimized g-values for the Cys-Tyr$^\bullet$ ($g_x = 2.0072$, $g_y = 2.0063$, $g_z = 2.0024$) are close to those previously reported from a high-field EPR investigation of this free radical ($g_x = 2.00741$, $g_y = 2.00641$, $g_z = 2.00211$) (*10*). The axial symmetry of the electronic g-tensor is a distinctive feature of the ground state for the thioether-substituted phenoxyl, very different from the strongly rhombic distortion that is characteristic of a simple tyrosyl phenoxyl free radical (*2, 3*). The latter is well documented in biological systems and is also observed in the high-power free radical EPR signal in oxidized apoGAOX (*vide infra*). Computational studies have indicated that the near-axial symmetry of the g-tensor for the Cys-Tyr$^\bullet$ free radical may be accounted for as a consequence of unpaired electron density in the sulfur valence shell (*10, 23*). Spin−orbit mixing contributions to the g-shifts from unpaired electron density localized on the exocyclic sulfur atom partially cancel the contributions from unpaired electron density on the phenoxyl oxygen, leading to a more axial g-tensor (*10*). This interpretation implies that a substantial fraction of the unpaired electron density resides on sulfur. Alternatively, the axial g-tensor has been ascribed to smaller spin−orbit and angular momentum matrix elements of the nπ^* excitation in the sulfur-substituted free radical, consistent with a negligible contribution of sulfur in the electronic ground state (*36*). The present analysis of the pattern of unpaired electron density in the Cys-Tyr$^\bullet$ free radical allows these conflicting descriptions to be evaluated in light of new experimental data.

A Lorentzian line shape is required to reproduce the shape of the spectra for the deuterated Cys-Tyr$^\bullet$ free radical, particularly in the low- and high-field tails. Lorentzian (homogeneously broadened) line shapes are relatively unusual in biological systems, where distributions over structural parameters (bond angles, distances) and solvation effects typically result in inhomogeneous line broadening (Gaussian line shape). However, the requirement for Lorentzian line shape is consistent with the relatively large inhomogeneity factor (b) required to fit the power saturation data (Figure 5), a value close to the Lorentzian limit. This suggests a relatively rigid structure for the Cys-Tyr$^\bullet$ cofactor in oxidized apoGAOX. The residual line width that is required to fit this spectrum, when the hyperfine contributions from the five ^{2}H nuclei derived from the tyrosine side chain are taken into account, is nearly isotropic and close to 2 G ($\Gamma_x = 2.0$ G, $\Gamma_y = 2.1$ G, $\Gamma_z = 2.5$ G). Unresolved ^{1}H hf splitting from the H_β protons on the Cys228 side chain (Figure 2) may be expected to contribute to this line width through coupling to the unpaired electron localized on S (Figure 2). This contribution may be estimated at approximately 2 G based on the experimentally determined spin density on sulfur (*vide infra*).

In contrast to the Lorentzian line shape required to simulate the low-power Cys-Tyr$^\bullet$ EPR signal, the high-power signal in oxidized apoGAOX may be fit with a Gaussian line shape. The g-tensor for the high-power species is also distinct ($g_x = 2.0101$, $g_y = 2.0062$, $g_z = 2.0022$), exhibiting the strong rhombic splitting characteristic of simple, unsubstituted tyrosyl phenoxyl.

^{1}H Hyperfine Parameters. Replacement of all ring hydrogens by deuterium (Figure 3b) results in a significant perturbation of the EPR spectrum (Figure 7b) compared to unlabeled oxidized apoGAOX (Figure 7a), due to the reduction in hf interactions associated with the smaller magnetogyric ratio of the ^{2}H nucleus. The spectral splittings are then dominated by interactions with the β-hydrogen of the tyrosyl side chain (Figure 2). The self-consistent hf parameters refined for the two H_β nuclei are given in Table 1 (columns 3−5).

Unambiguous assignment of the H_β hf parameters through analysis of selectively deuterated samples resolves inconsistencies in the assignments reported in previous EPR studies

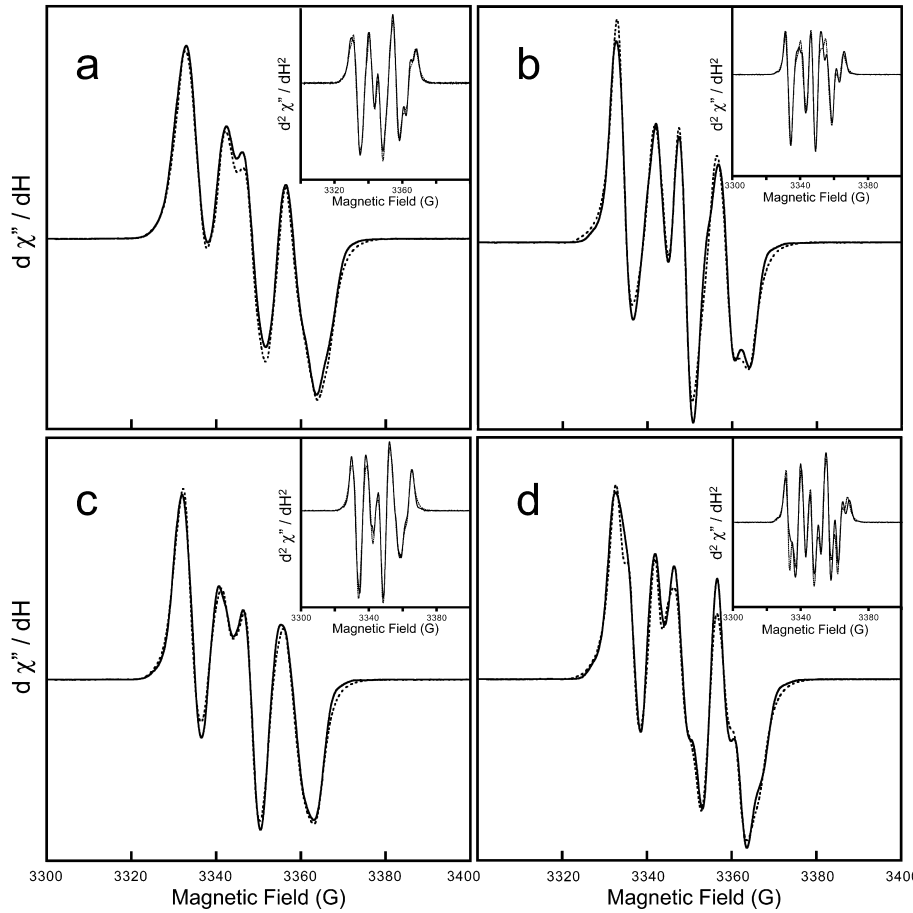

FIGURE 7: EPR spectra for $^{1}H/^{2}H$ isotopic variants of apoGAOX free radical. Oxidized apoGAOX in 25 mM $KHPO_4$ buffer, pH 7: (a) unlabeled (1.3 mM protein); (b) [2,2′,3′,5′,6′-$^{2}H_5$]-DL-tyrosine (1.1 mM protein); (c) [3′,5′-$^{2}H_2$]-L-tyrosine (1.1 mM protein); (d) [2,2′,6′-$^{2}H_3$]-DL-tyrosine (1.4 mM protein). Inset: Second derivative EPR spectra. (Dashed line) XSophe simulation as described in the Experimental Procedures using the parameters in Table 1. Instrumental parameters: microwave power, 50 μW; microwave frequency, (a) 9.399 GHz, (b) 9.396 GHz, (c) 9.395 GHz, (d) 9.400 GHz; modulation frequency, 1 G; temperature, 100 K.

Table 1: Experimental and Theoretical Electron-Nuclear Hyperfine Parameters for Cys-Tyr• Free Radical

		A^a (G)							theoretical		
label	atom	A_{xx} (G)	A_{yy} (G)	A_{zz} (G)	$A_{iso}{}^c$ (G)	$T_{zz}{}^d$ (G)	$A_{iso}{}^e$ (G)	$T_{zz}{}^e$ (G)	$A_{iso}{}^f$	$A_{iso}{}^g$	$A_{iso}{}^h$
^{1}H	α-2′	0.37	2.24	0.79	1.13	−0.34	0.39		2.7	1.5	2.8
	α-5′	−1.55[b]	−4.15	−3.07	−2.92	−0.14	−0.95		−5.7	−4.9	−5.7
	α-6′	2.32	0.24	0.70	1.09	−0.38	0.62		1.7	0.0	1.7
	β-1	13.8	15.0	13.9	14.2	−0.34	14.9		−18		
	β-2	8.6	9.7	7.7	8.64	−1.0	7.17				
^{13}C	C-1′	0.1	0.4	24	8.16	15.83	7.22	20.7			15.4
	C-2′	−6.2	−4.9	−7.2	−6.1	−1.1	−6.52	−1.21			−9.6
	C-3′	1.4	1.1	20.3	7.6	12.7	8.36	12.5			12.3
	C-4′	−7.7	−6.2	−2.1	−5.35	3.2	−5.40	3.11			−7.9
	C-5′	1.7	1.7	4.5	2.65	1.87	0.91	2.91			8.6
	C-6′	−3.5	−2.8	−5.7	−4.0	−1.7	−5.04	−1.90			−7.1
^{17}O	O	2.5	3	−30	−8.17	−21.8	−7.36	−22.1			−9.6
^{33}S	S	−2.25	−1.67	17.8	4.63	13.2	5.18	12.5			1.6

[a] Total hyperfine interaction evaluated by iterative simulation of the entire set of spectra from isotopomeric GAOX derivatives as described in the Experimental Procedures. [b] Sign ambiguity resolved by reference to values for tyrosyl phenoxyl free radical. [c] $A_{iso} = (A_{xx} + A_{yy} + A_{zz})/3$. [d] $T_{zz} = A_{zz} - A_{iso}$. [e] Calculated from the consensus spin distribution (Table 2) using the hyperfine coupling models. [f] For (2-methylthio)cresyl phenoxyl free radical (MTC•) from ref *21* (B3LYP functional). [g] For MTC• free radical from ref *21* (PWP86 functional). [h] For MTC• free radical from ref *22* [B3LYP functional/6-31G(d) basis set].

on the Cys-Tyr• free radical in galactose oxidase (*9, 10*). Earlier ENDOR (*9*) and high-frequency EPR (*10*) experiments correctly assigned a nearly isotropic 14.5 G hf interaction to one of the H_β protons. However, the more anisotropic splitting with A_{iso} near 9 G was assigned in the former case to a ring H_α proton and in the latter case to a H_β associated with the Cys228 side chain. The present results provide a definitive assignment of the two side chain H_β hydrogen hf couplings, whose ratio is consistent with predictions based on the crystallographically observed headgroup geometry of the Cys-Tyr cofactor (Figure 2b).

Simulation of the high-power spectrum for protein labeled with ring-deuterated tyrosine yields estimates of the corresponding hyperfine parameters for the secondary free radical species, which are nearly identical with those found for the

Table 2: Experimental and Theoretical Electron Spin Distributions for Cys-Tyr• Free Radical

atom	ρ_{exp}[a]	ρ_{calc}[c]	ρ_{calc}[d]	ρ_{calc}[e]	ρ_{calc}[f]
C-1′	0.27	0.35	0.34	0.28	0.32
C-2′	−0.02	−0.16	−0.16	−0.09	−0.12
C-3′	0.16	0.28	0.28	0.21	0.24
C-4′	0.04	−0.06	−0.06	0.02	−0.02
C-5′	0.04	0.23	0.23	0.18	0.20
C-6′	−0.03	−0.11	−0.11	−0.03	−0.07
O	0.18	0.35	0.35	0.28	0.31
S	0.23[b]	0.11	0.11	0.15	0.14
Σ	0.9	1.0	1.0	1.0	1.0

[a] Evaluated as described in the Results and Discussion. [b] A range of values (0.17−0.23) is obtained for ρ_{exp}(S) depending on the value of Qs used (eq 19). [c] For MTC• free radical from ref *22* [B3LYP functional/6-31G(d) basis set]. [d] For MTC• free radical from ref *21* (B3LYP functional). [e] For MTC• free radical from ref *21* (PWP86 functional). [f] For MTC• free radical from ref *23* (BP86 functional).

low-power species. This information limits the possible sites of the secondary free radical species in the protein structure.

Selective substitution of the ring hydrogens by deuterium (Figure 3c,d) also affects the Cys-Tyr• EPR spectrum, but more subtly (Figure 7c,d). These changes allow the magnitude of the hf parameters for the ring hydrogens to be estimated (Table 1). Hyperfine tensors for H_α ring protons are likely to be quite rhombic and noncoaxial with the *g*-tensor, generally being oriented along the C−H bond vector (*24*). Thus, as a first approximation, the orientation of the hyperfine tensors for the ring protons was defined accordingly (Supporting Information, Figure S1). The unique hydrogen *ortho* to the phenol oxygen allows the hf parameters for the H_α-5′ position to be assigned unambiguously. In contrast, the 2′ and 6′ positions cannot be distinguished in these experiments, and additional information is required to make the assignment (*vide infra*).

^{13}C Hyperfine Parameters. Selective substitution of ring carbon atoms by ^{13}C provides a relatively direct probe of the unpaired electron density at each of the ring positions through the magnitude of the anisotropic hyperfine coupling (*vide infra*). Three substitution patterns (Figure 3f−h) were used to determine the hf parameters for all six ring carbons. The hf parameters obtained for the [4-^{13}C]tyrosine derivative (Figure 3f) may be uniquely assigned to the C-4′ (phenoxyl) position, since it is the only position labeled in that isotopomer (Figure 8a). The doubly labeled [3′,5′-$^{13}C_2$]tyrosine yields a Cys-Tyr• that contains the isotopic probe in two structurally distinct positions: the 3′ position (the site of the C−S covalent bond) and the 5′ position (attached to a ring hydrogen) (Figure 3g). While these two positions are symmetrical and equivalent in an unmodified tyrosine ring system, they are inequivalent in the Cys-Tyr structure. This implies that the hf parameters are likely to be distinct, and the spectral simulations do, in fact, require two hf tensors to satisfactorily reproduce the observed features (Figure 8b). Assignment of the two hf tensors to one or other position is clearly a problem, which we have addressed by correlating ^{13}C and ^{1}H hf data. Specifically, the hf parameters for the unique H_α-5′ are particularly sensitive to the unpaired spin density at the neighboring carbon, and the ^{13}C-5′ hf tensor should be consistent with those results. This allows assignment of the two ^{13}C hf tensors (Table 1).

Hyperfine parameters associated with the remaining three ring positions (1′, 2′, 6′) (Figure 3h) were evaluated by fixing the parameters for the 3′, 4′, and 5′ positions (determined above) during the simulation of the EPR spectrum obtained for the [U-$^{13}C_6$]tyrosine derived Cys-Tyr• (Figure 8c). Consistent with a moderately perturbed typical tyrosyl odd-alternant spin distribution, one of the hf tensors has a relatively large magnitude. This tensor may be assigned to the C-1′ position, which is predicted to bear a relatively large fraction of the unpaired electron density. This prediction is also supported by the magnitude of the C_β−H hf interactions, which also report on unpaired spin density at the C-1′ position (*vide infra*). This correlation permits unambiguous assignment of one of the three hf tensors. The other two hf tensors are quite similar (Table 1), and a definitive assignment is not required for the remaining analysis.

^{17}O Hyperfine Parameters. The unique oxygen in the tyrosine side chain was substituted by the paramagnetic isotope ^{17}O in order to probe the oxygen valence contributions to unpaired electron distribution in the Cys-Tyr• free radical (Figure 3i). In this case the enrichment of the isotope was relatively low (50 atom % ^{17}O), resulting in a strong signal from the unlabeled fraction containing the natural abundance isotope, ^{16}O ($I = 0$) (Figure 8d). Hyperfine splitting from the high-spin ($I = {}^5/_2$, $\gamma_{^{17}O} = -3.62806 \times 10^7$ rad s^{-1} T^{-1}) nucleus of the ^{17}O isotope spreads the EPR spectrum of the labeled fraction over a very wide magnetic field range (300 G). Fitting the resulting spectrum with the actual isotope distribution (Figure 8d) yields a high quality simulation that allows the ^{17}O hf parameters to be evaluated (Table 1).

^{33}S Hyperfine Parameters. Substitution of the paramagnetic isotope ^{33}S ($I = {}^3/_2$, $\gamma_{^{33}S} = 2.055685 \times 10^7$ rad s^{-1} T^{-1}) for nonmagnetic ^{32}S and ^{34}S isotopes (combined 99.2% n.a.) in the Cys-Tyr cofactor (Figure 3j) permits the contribution of the thioether sulfur to the ground state unpaired electron distribution to be experimentally measured. This is clearly a critical aspect of the characterization of the Cys-Tyr• free radical. The EPR spectrum of the ^{33}S-labeled Cys-Tyr• free radical (Figure 9) is broadened and exhibits additional hyperfine splittings, compared to the spectrum of the unlabeled protein (Figure 7a). Simulation of the ^{33}S-perturbed spectrum yielded estimates of the hf tensor components (Table 1).

These experimental electron-nuclear hyperfine data may be compared with values obtained from density functional calculations of the electronic ground state of the (2-methylthio)cresyl phenoxyl (MTC•) free radical (a simplified model for Cys-Tyr• free radical) in the literature (Table 1). One of the calculations (*21*) only reports proton hf coupling constants, which are relatively uninformative probes of the electronic structure. The calculations correctly describe the general pattern of hf interactions for H_α protons, which in turn reflects the overall odd-alternant spin distribution for the π-radical. However, the magnitude of the hf coupling to the H_α-5′ ring proton is significantly overestimated. Further, where hf parameters for C, O, and S are reported (*22*), the calculations systematically overestimate the value of A_{iso} for ^{17}O and ring carbons and underestimate the value for ^{33}S. It is not clear whether this computational work was influenced by the large hf coupling constant previously (incorrectly) assigned to H_α-

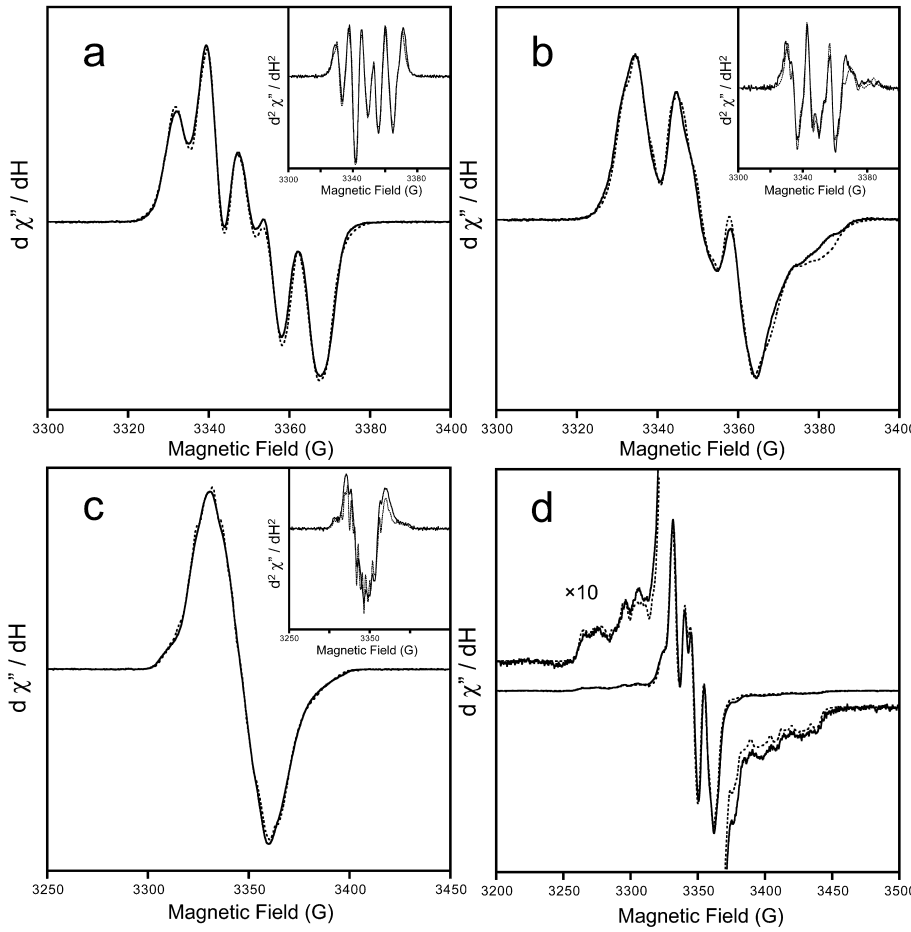

FIGURE 8: EPR spectra for ^{13}C and ^{17}O isotopic variants of apoGAOX free radical. Oxidized apoGAOX in 25 mM $KHPO_4$ buffer, pH 7: (a) [4′-^{13}C]-L-tyrosine (0.8 mM protein); (b) [3′,5′-$^{13}C_2$]-L-tyrosine (0.9 mM protein); (c) [ring-$^{13}C_6$]-L-tyrosine (1.2 mM protein); (d) ([4′-^{17}O]-L-tyrosine (0.8 mM protein). Inset: Second derivative EPR spectra. (Dashed line) XSophe simulation as described in the Experimental Procedures using the parameters in Table 1. Instrumental parameters: microwave power, 50 μW; microwave frequency, (a) 9.405 GHz, (b) 9.411 GHz, (c) 9.395 GHz, (d) 9.394 GHz; modulation frequency, 1 G; temperature, 100 K.

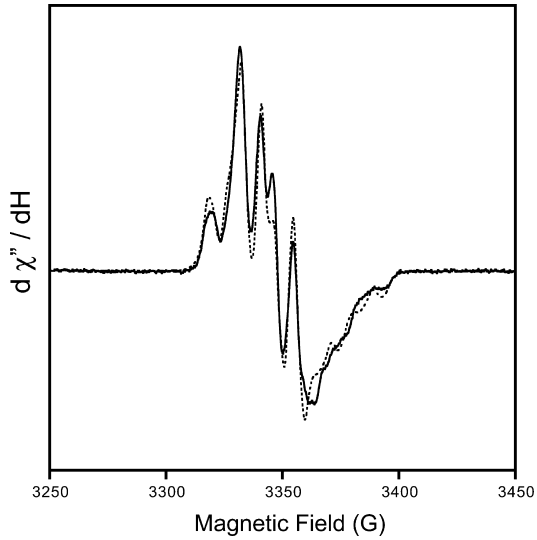

FIGURE 9: EPR spectrum for the ^{33}S isotopic variant of apoGAOX free radical. Oxidized apoGAOX labeled with ^{33}S in 25 mM $KHPO_4$ buffer, pH 7 (0.45 mM protein). (Dashed line) XSophe simulation as described in the Experimental Procedures using the parameters in Table 1. Instrumental parameters: microwave power, 50 μW; microwave frequency, 9.406 GHz; modulation frequency, 1 G; temperature, 100 K.

5′ based on ENDOR experiments (*9*). As described above, this hf interaction is now definitively assigned to the second H_β of the tyrosine side chain (Figure 2) rather than to H_α-5′. It appears that the unexpectedly small hf parameters for H_α-5′, assigned experimentally by selective deuterium substitution at this unique position,are not consistent with theoretical predictions that require a very small thioether perturbation to the Cys-Tyr• ground state. This analysis is extended by a reconstruction of the spin distribution of the Cys-Tyr• free radical in the following section.

Spin Density Reconstruction. The experimental isotropic and dipolar hf parameters (Table 1, columns 6 and 7, obtained as described above) serve as the starting point for analysis of the unpaired electron distribution giving rise to these interactions. The approach used here makes use of local electronic structure models developed to describe the origins of hf interactions in delocalized π-radicals based on experimentally calibrated dipolar tensors and semiempirical Q coefficients (proportionality constants relating the magnitude of the unpaired spin density on atoms within the π-system to individual A_{iso} hf values) describing the spin polarization behavior for pairs of bonded atoms (eqs 8–20, below) (*37*). We make use of these models to assign spin density to specific sites within the Cys-Tyr framework.

The electronic structure of the Cys-Tyr• free radical is expected to be similar to the simple tyrosyl phenoxyl free

radical from which it is derived. The latter free radical has been the subject of a wide range of theoretical (*24*) and experimental (*24–26*) studies. The single unpaired electron of the tyrosyl free radical is delocalized over the entire conjugated π-system, with spin density present mainly in the p_z orbitals perpendicular to the ring plane. The tyrosyl free radical exhibits a distinctive odd-alternant spin distribution, resulting from the nodal character of the highest occupied molecular orbital (SOMO). This pattern localizes the unpaired electron mainly on three ring carbons (C-1′, C-3′, and C-5′) and on the phenoxyl oxygen. A similar pattern is predicted for the Cys-Tyr$^\bullet$ free radical, but in the latter case an additional contribution from the thioether sulfur of the covalent cross-link (Figure 2) has to be considered. Thus, eight local spin density terms (ρ_X^π) must be determined for the eight (C, O, S) nuclei (X) contributing to the π-system in order to define the pattern of spin density in the Cys-Tyr$^\bullet$ ground state.

The unpaired spin distribution interacts with magnetic nuclei (^{1}H, ^{2}H, ^{13}C, ^{17}O, or ^{33}S) via two distinct mechanisms (*37*). Through-bond spin polarization effects lead to a purely isotropic, Fermi contact contribution to the hf interaction (*37, 38*), described by the isotropic hf tensor, A_{iso}. In addition, dipole−dipole (through-space) interactions depend primarily on geometry and contribute to the purely anisotropic part of the hf interaction, the dipolar tensor, $\boldsymbol{T}$. Spin polarization also induces minority (β, negative) spin density through spin-dependent exchange interactions, making the sum of the absolute values of atom-centered unpaired spin in the electronic structure greater than unity, even in a free radical with a single unpaired electron (*38*). Thus, while the majority (α, positive) spin density more or less reflects the distribution of electron density in the SOMO, oppositely signed β spin density is induced on neighboring atoms. As a result, in general the sum of α spin density over all atoms is greater than one, although the sum over both α and β spins must be unity ($\sum_{atoms}(\rho_\alpha + \rho_\beta = 1)$).

In a spin system as complex as the Cys-Tyr$^\bullet$ free radical, the ρ_X^π value generally cannot be evaluated directly from the hf tensor of an individual atom X, because spin polarization makes significant contributions to the hf interactions at neighboring atoms. Theoretical models for these local spin polarization terms have been developed and used successfully to interpret the isotropic hf constants for EPR spectra of a wide range of π-radicals. One of the best known of these expressions is the McConnell equation for a β-proton vicinal to a π-radical (eq 8) (*39*):

$$A_C^{H_\beta} = B_2 \rho_{C\text{-}1'}^\pi \cos^2\theta \tag{8}$$

where $A_C^{H_\beta}$is the isotropic part of the hf interaction for the β-proton ($A_{iso} = (A_{xx} + A_{yy} + A_{zz})/3$), B_2 is a constant (58 G) reflecting the magnitude of the Fermi contact interaction at the β-proton for unit spin on C-1′, $\rho_{C\text{-}1'}^\pi$ is the fractional unpaired spin in the $2p_z$ orbital on C-1′, and θ is the dihedral angle of the C−H_β bond vector relative to the p_z orbital axis (Figure 2). Orientation-independent contributions to the hyperfine interaction (including spin polarization) are considered to be relatively small for β-protons and are neglected in eq 8. In a protein where the dihedral angles between the geminal β-protons may be considered fixed at 120° and both β-proton hf interactions are determined by the same value of $\rho_{C\text{-}1'}^\pi$ on C-1′, experimental evaluation of the two A_{iso}^H values allows both $\rho_{C\text{-}1'}^\pi$ and the dihedral angles (θ and θ') to be determined. This approach has been elegantly developed in a recent paper by Svistunenko and Cooper (*40*). Application of this method using data for the Cys-Tyr$^\bullet$ free radical (Table 1) leads to predicted values $\theta = 18°$ and $\rho_{C\text{-}1'}^\pi = 0.27$. For comparison, the crystal structure of metal-free apoGAOX (PDB ID 1goh) indicates a headgroup dihedral $\theta = 12.5°$ (Figure 2b).

Interestingly, the H_β hf parameters for the secondary free radical species detected at high power are nearly identical to those observed for the Tyr-Cys$^\bullet$ free radical. On the basis of the McConnell equation (eq 8), this implies the same dihedral geometry for both tyrosyl side chains, allowing the potential sites for localization of the secondary free radical to be determined from the crystal structure, as suggested by Svistunenko and Cooper (*40*). Analysis of the structure of apoGAOX (PDB ID 1goh) indicates that the majority of the 24 tyrosine residues in the protein adopt a distinct conformation, with the headgroup dihedral in the range $\theta = 35-60°$. Only two residues (Tyr272, Tyr532) exhibit a headgroup dihedral near $\theta = 12°$, consistent with the present EPR data. This suggests two possibilities: that the secondary free radical represents a small fraction of the protein that is not cross-linked or that Tyr532, which is remote from the active site, is capable of stabilizing a free radical. The higher relaxivity of the secondary radical suggests a distinct protein environment, possibly associated with greater phenoxyl mobility, greater solvent perturbation, or interaction with a paramagnetic center such as an adventitious metal ion. More precise characterization of the secondary free radical will require mutagenesis of each of the potential sites.

Dipolar coupling between the π-electron spin density at C-1′ and the β-protons is relatively small and essentially independent of the side chain dihedral and is given by eq 9 (*24*):

$$T_{H_\beta} = \begin{bmatrix} 0.7 & 0 & 0 \\ 0 & -0.3 & 0 \\ 0 & 0 & -0.4 \end{bmatrix} \rho_{C\text{-}1'}^\pi \tag{9}$$

with principal components (T_{xx}, T_{yy}, and T_{zz}) in gauss.

The unpaired spin density associated with the π-bonding system of the tyrosine ring also gives rise to hf interactions with ring hydrogens (H_α) through a spin polarization mechanism, the magnitude of the interaction being dominated by the spin density on the carbon atom to which the hydrogen is bonded. The McConnell equation describing this interaction is (eq 10) (*41*):

$$A_C^{H_\alpha} = Q_{CH}^H \rho_C^\pi \tag{10}$$

Here Q_{CH}^H describes the $\sigma-\pi$ overlap contributions to spin polarization at the hydrogen nucleus. Previous studies on tyrosyl free radicals have estimated a value of −24.9 G for Q_{CH}^H (*24*).

Hyperfine interactions for (^{13}C) ring carbon atoms include both dipolar (anisotropic) contributions (dominated by the unpaired spin density in the $2p_z$ orbital of the same atom) and the isotropic (Fermi contact) contributions that are also sensitive to the unpaired spin density on neighboring atoms,

a consequence of $\sigma-\pi$ polarization effects. The dipolar term is relatively simple (eq 11) (*24, 42*):

$$T_C = \begin{bmatrix} -38.3 & 0 & 0 \\ 0 & -38.3 & 0 \\ 0 & 0 & 76.6 \end{bmatrix} \rho_C^\pi \quad (11)$$

This expression describes the hf coupling between a ^{13}C nucleus and unpaired spin density in the $2p_z$ orbital on the same atom, with the magnitude of the tensor components reflecting the magnitude of the magnetogyric ratio for the ^{13}C nucleus and the radial part of the $C(2p_z)$ wave function (*42*). In general, this expression can be expanded to include a sum over neighboring atoms in order to account for dipolar coupling at atoms with low spin density.

The isotopic hf interactions are best described by the Karplus−Fraenkel equation (*43*), which parametrizes $\sigma-\pi$ orbital mixing terms over neighboring atoms contained within a conjugated π-system (eq 12):

$$A_C^C = \left(S^C + \sum_{i=1}^{3} Q_{CX_i}^C\right)\rho_C^\pi + \sum_{i=1}^{3} Q_{X_iC}^C \rho_{X_i}^\pi \quad (12)$$

where S^C reflects the 1s contributions and the Qs describe the 2s contributions. The values of S^C and the Qs have been estimated using semiempirical computational methods and calibrated using experimental EPR data. The values −18.75, 14.44, −13.94, and 19.5 G are used in the present study for S^C, $Q_{CC'}^C$, $Q_{C'C}^C$, Q_{CH}^C, respectively (*43*). This approach provides a method for estimating the contribution of local spin density distribution to the hf interactions based on molecular fragments, regardless of the overall structure of the free radical. Karplus−Fraenkel theory leads to a set of equations for the isotopic hf interactions for each of the ring carbons (eqs 13–16):

$$\text{C-1}'\text{:}\quad A_{C\text{-}1'}^C = (S^C + 3Q_{CC'}^C)\rho_C^\pi + Q_{C'C}^C(\rho_{C'}^\pi + \rho_{C''}^\pi + \rho_{C'''}^\pi) \quad (13)$$

$$\text{C-2}', \text{C-5}', \text{C-6}'\text{:}\quad A_{C\text{-}2'}^C = (S^C + 2Q_{CC'}^C + Q_{CH}^C)\rho_C^\pi + Q_{C'C}^C(\rho_{C'}^\pi + \rho_{C'}^\pi) \text{ etc.} \quad (14)$$

$$\text{C-3}'\text{:}\quad A_{C\text{-}3'}^C = (S^C + 2Q_{CC'}^C)\rho_C^\pi + Q_{C'C}^C(\rho_{C'}^\pi + \rho_{C''}^\pi) + Q_{CS}^C\rho_C^\pi + Q_{SC}^C\rho_S^\pi \quad (15)$$

$$\text{C-4}'\text{:}\quad A_{C\text{-}4'}^C = (S^C + 2Q_{CC'}^C)\rho_C^\pi + Q_{C'C}^C(\rho_{C'}^\pi + \rho_{C''}^\pi) + Q_{CO}^C\rho_C^\pi + Q_{OC}^C\rho_O^\pi \quad (16)$$

The expressions for A_{iso} for ring positions C-3′ and C-4′ include $\sigma-\pi$ mixing terms for the C−O and C−S bonds, respectively. The values used for Q_{CO}^C, Q_{OC}^C, Q_{CS}^C, and Q_{SC}^C were 36, −24.3, 1.8, and 30 G, respectively (*44, 45*).

The unpaired spin density on the phenoxyl oxygen is reflected in the magnitude of the hf coupling to the ^{17}O nucleus in the isotopically substituted Cys-Tyr cofactor (Figure 3g). The expression for the isotropic hf interaction includes spin polarization terms for unpaired spin density on both oxygen and the covalently bonded ring carbon (eq 17) (*24, 44*):

$$A_O^O = Q_{OC}^O\rho_O^\pi + Q_{CO}^O\rho_{C\text{-}4'}^\pi \quad (17)$$

The values for the $\sigma-\pi$ mixing terms (Q_{OC}^O and Q_{CO}^O) were −40 and 0 G, respectively (*24, 44*). The dipolar coupling expression for unpaired spin density in the $2p_z$ orbital on oxygen, scaled by the magnitude of the radial part of the $O(2p_z)$ wave function and the nuclear magnetogyric ratio, is (eq 18)

$$T_O = \begin{bmatrix} 60 & 0 & 0 \\ 0 & 60 & 0 \\ 0 & 0 & -120 \end{bmatrix} \rho_O^\pi \quad (18)$$

where ρ_O^π is the spin density in the $2p_z$ orbital on oxygen, the tensor components are in units of gauss, and the sign of the magnetogyric ratio for ^{17}O is reflected in the sign of the tensor components.

A similar set of equations holds for the thioether sulfur (*45–49*). A simple expression has been proposed for the isotropic part (eq 19):

$$A_S^S = Q_S\rho_S^\pi \quad (19)$$

where Q_S includes both s- and p-orbital contributions, with literature values ranging from 23 to 33 G (*46, 47*). The dipolar contribution takes the form (eq 20):

$$T_S = \begin{bmatrix} -27.8 & 0 & 0 \\ 0 & -27.8 & 0 \\ 0 & 0 & 55.6 \end{bmatrix} \rho_S^\pi \quad (20)$$

Taken together, these expressions generate a set of 21 simultaneous equations in the 8 unknown atomic π spin densities (ρ_X^π) for the Cys-Tyr• free radical. Using global fitting parameter minimization methods, it was possible to solve the 21 simultaneous equations relating the (experimentally determined) hf parameters to the spin densities (ρ_X^π) (eqs 8–20). This approach yields optimized, best-fit values of the atomic spin densities (Table 2), associated with a modified set of hf values (Table 1, columns 8 and 9) corresponding to the consensus spin density distribution.

As expected, the pattern of unpaired electron spin reconstructed from the hf parameters (Table 2) strongly resembles the odd-alternant distribution predicted theoretically for phenoxyl free radicals, and demonstrated experimentally for simple tyrosyl free radicals, with large alternating unpaired spin densities on the ring carbons and the phenoxyl oxygen. However, there are significant differences from the simple tyrosyl free radical. First, the unpaired spin localized on C-1′ is relatively small. This result is reflected in both the magnitude of the C_β−H hf interactions and in the C-1′ ^{13}C hf coupling. The reduction in spin density at C-1′ (and other positions) must reflect a corresponding buildup of spin density at some other site(s). Similar reduction in spin density (relative to the simple tyrosyl free radical model systems) is observed for the other ring carbons, as well as for the phenoxyl oxygen. On the other hand, the magnitude of both isotropic and anisotropic hf interactions of the ^{33}S nucleus indicates a substantial fraction of unpaired spin density is localized in the valence orbital of the thioether sulfur in the Cys-Tyr• free radical.

The experimentally determined spin density on sulfur is at the higher end of the range estimated in recent calculations of the electronic structure of the Cys-Tyr• free radical (*10, 20–23*). The value is consistent with earlier interpretation of the origins of the axial electronic *g*-tensor from compensating oxygen and sulfur valence contributions to the *g*-shift (*10, 23*). This provides clear evidence for delocalization of the

unpaired electron onto the thioether side chain. It is also consistent with the magnitude of the residual line width observed for Cys-Tyr• derived from perdeuterated tyrosine (Figure 6). On the basis of the C−H bond dihedrals observed for the Cys228 headgroup geometry determined crystallographically ($\theta = 73°$) (Figure 2), and the experimental sulfur spin density, an isotropic hf coupling of ~2 G is predicted for the Cys228 β-protons based on the McConnell equation (eq 8), consistent with the magnitude of the residual line width observed in the apoGAOX free radical labeled with perdeuterated tyrosine (Figure 6).

The calculated ^{33}S hyperfine coupling constants reported in Table 1, associated with a value for the sulfur contribution to the unpaired spin density $\rho_S^\pi = 0.23$, slightly overestimate A_{iso} (1.12×) and underestimate the dipolar coupling T_{zz} (0.95×). The value of Q_S used for evaluation of A_{iso} (Q_S = 23 G) is the smaller of two values reported in the literature. The larger value (Q_S = 33 G) has been successfully applied to interpreting sulfur spin densities in thiaheterocyclic free radicals (*46*), while the smaller value (Q_S = 23 G) has been proven useful in the analysis of arylthioaminyl free radicals (*47*). However, neither has been specifically evaluated for thioether substituents of the type present in the Cys-Tyr cofactor. The larger value would reproduce the experimental A_{iso} value with ρ_S^π as small as 0.17, but the dipolar coupling (T_{zz}) for the sulfur nucleus would then be more significantly underestimated (0.87×). Thus, the experimental data are consistent with a range of sulfur spin density (ρ_S^π = 0.17−0.23) similar to the amount of spin density localized on the phenoxyl oxygen in the Cys-Tyr• free radical (ρ_O^π = 0.18), representing a substantial contribution to the ground state electronic structure.

CONCLUSIONS

A systematic isotopic perturbation of the Cys-Tyr• free radical by site-selective labeling has allowed us to extract nuclear hyperfine parameters used to reconstruct the unpaired spin distribution in the electronic ground state. The result indicates an unexpectedly small unpaired electron density on the 5′ carbon, associated with a small hyperfine interaction for the neighboring H_α-5′ ring hydrogen (Table 1). The small value of the H_α-5′ hyperfine coupling is consistent with solution EPR data previously reported for the (2-methylthio)cresyl (MTC•) model free radical, yielding $|A_{iso}| = 3.1$ G for H_α-5′ (*11*), close to the value we have obtained (2.9 G). These values are less than half the magnitude of A_{iso} observed for the corresponding H_α-5′ hydrogen in a simple tyrosyl phenoxyl free radical (7 G), indicating a shift in the unpaired electron distribution. Analysis of the EPR spectrum of ^{33}S-labeled Cys-Tyr• in galactose oxidase demonstrates a significant unpaired spin density resides on the thioether cross-link. Nearly equal amounts of unpaired spin density (~0.2) are localized on the thioether sulfur and the phenoxyl oxygen in Cys-Tyr• free radical, reflecting a substantial perturbation of the electronic ground state relative to a Tyr• free radical. The effect of this electronic structural perturbation on the reactivity of the Cys-Tyr cofactor may be reflected in its lower O−H bond dissociation energy in its reduced form, facilitating hydrogen atom donation to O_2 during catalysis (*50*), and in the unusually low redox potential of the cofactor, allowing the protein to stabilize a free radical under mild conditions.

SUPPORTING INFORMATION AVAILABLE

Figure S1 defining the orientation of hyperfine tensors used in the XSophe simulations for Hα ring protons. This material is available free of charge via the Internet at http://pubs.acs.org.

REFERENCES

1. Frey, P. A., Hegeman, A. D., and Reed, G. H. (2006) Free radical mechanisms in enzymology. *Chem. Rev. 106*, 3302–3316.
2. Stubbe, J. (2003) Di-iron-tyrosyl radical ribonucleotide reductases. *Curr. Opin. Chem. Biol. 7*, 183–188.
3. Pujols-Ayala, I., and Barry, B. A. (2004) Tyrosyl radicals in photosystem II. *Biochim. Biophys. Acta 1655*, 205–216.
4. Frey, P. A., and Booker, S. J. (2001) Radical mechanisms of S-adenosylmethionine-dependent enzymes. *Adv. Protein Chem. 58*, 1–45.
5. McPherson, M. J., Parsons, M. R., Spooner, R. K., and Wilmot, C. M. (2001) Galactose oxidase, in *Handbook of Metalloproteins* (Wieghart, K., Poulos, T. L., Huber, R., and Messerschmidt, A., Eds.) Vol. 2, pp 1245−1257, Wiley, New York.
6. Whittaker, J. W. (2003) Free radical catalysis by galactose oxidase. *Chem. Rev. 103*, 2347–2363.
7. Whittaker, M. M., and Whittaker, J. W. (1990) A tyrosine-derived free radical in apogalactose oxidase. *J. Biol. Chem. 265*, 9610–9613.
8. Ito, J., Philips, S. E., Stevens, C., Ogel, Z. B., McPherson, M. J., Keen, J. N., Yadav, K. D., and Knowles, P. F. (1991) Novel thioether bond revealed by a 1.7 Å crystal structure of galactose oxidase. *Nature 350*, 87–90.
9. Babcock, G. T., El-Deeb, M. K., Sandusky, P. O., Whittaker, M. M., and Whittaker, J. W. (1992) Electron paramagnetic resonance and electron nuclear double resonance spectroscopies of the radical site in galactose oxidase and thioether-substituted phenol model compounds. *J. Am. Chem. Soc. 114*, 3727–3734.
10. Gerfen, G. J., Bellew, B. F., Griffin, R. G., Singel, D. J., Ekberg, C. A., and Whittaker, J. W. (1996) High-frequency electron paramagnetic resonance spectroscopy of the apogalactose oxidase radical. *J. Phys. Chem. 100*, 16739–16748.
11. Itoh, S., Takayama, S., Arakawa, R., Furuta, A., Komatsu, M., Ishida, A., Takamuku, S., and Fukuzumi, S. (1997) Active site models for galactose oxidase. Electronic effect of the thioether group in the novel cofactor. *Inorg. Chem. 36*, 1407–1416.
12. Rogers, M. S., Baron, A. J., McPherson, M. J., Knowles, P. F., and Dooley, D. M. (2000) Galactose oxidase pro-sequence cleavage and cofactor assembly are self-processing reactions. *J. Am. Chem. Soc. 122*, 990–991.
13. Whittaker, M. M., and Whittaker, J. W. (2003) Cu(I)-dependent biogenesis of galactose oxidase redox cofactor. *J. Biol. Chem. 278*, 22090–22101.
14. Whittaker, M. M., Kersten, P. J., Cullen, D., and Whittaker, J. W. (1999) Identification of catalytic residues in glyoxal oxidase by targeted mutagenesis. *J. Biol. Chem. 274*, 36226–36232.
15. Whittaker, M. M., and Whittaker, J. W. (2006) *Streptomyces coelicolor* oxidase (SCO2387p): A new free radical metalloenzyme secreted by *Streptomyces coelicolor* A3(2). *Arch. Biochem. Biophys. 452*, 108–118.
16. Simmons, C. R., Lu, Q., Huang, Q., Hao, Q., Begley, T. P., Karplus, P. A., and Stipanuk, M. H. (2006) Crystal structure of mammalian cysteine dioxygenase. *J. Biol. Chem. 281*, 18723–18733.
17. Ye, S., Wu, X., Wei, L., Tang, D., Sun, P., Bartlam, M., and Rao, Z. (2007) An insight into the mechanism of the human cysteine dioxygenase. Key roles of the thioether bonded tyrosine-cysteine cofactor. *J. Biol. Chem. 282*, 3391–3402.
18. Schnell, R., Sandalova, T., Hellman, Lindqvist, Y., and Schneider, G. (2005) Siroheme- and $[Fe_4S_4]$-dependent NirA from *Mycobacterium tuberculosis* is a sulfite reductase with a covalent Cys-Tyr bond in the active site. *J. Biol. Chem. 280*, 27319–27328.
19. Wright, C. R., and Sykes, A. G. (2001) Interconversion of Cu^I and Cu^{II} forms of galactose oxidase: comparison of reduction potentials. *J. Inorg. Biochem. 85*, 237–243.
20. Himo, F., Eriksson, L. A., Maseras, F., and Siegbahn, P. E. M. (2000) Catalytic mechanism of galactose oxidase: A theoretical study. *J. Am. Chem. Soc. 122*, 8033–8036.
21. Himo, F., Babcock, G. T., and Eriksson, L. A. (1999) Tyrosyl radical in galactose oxidase not strongly perturbed by cysteine cross-link. *Chem. Phys. Lett. 313*, 374–378.

22. Wise, K. E., Pate, J. B., and Wheeler, R. A. (1999) Phenoxyl, (methylthio)phenoxyl and (methylthio)cresyl radical models for the structures, vibrations, and spin properties of the cysteine-linked tyrosyl radical in galactose oxidase. *J. Phys. Chem. B 103*, 4764–4772.
23. Kaupp, M., Gress, T., Reviakine, R., Malkina, O. L., and Malkin, V. G. (2003) g Tensor and spin density of the modified tyrosyl radical in galactose oxidase: A density functional study. *J. Phys. Chem. B 107*, 331–337.
24. Hulsebosch, R. J., van den Brink, J. S., Nieuwenhuis, S. A. M., Gast, P., Raap, J., Lugtenburg, J., and Hoff, A. J. (1997) Electronic structure of the neutral tyrosine radical in frozen solution. Selective ^{2}H-, ^{13}C-, and ^{17}O-isotope labeling and EPR spectroscopy at 9 and 35 GHz. *J. Am. Chem. Soc. 119*, 8685–8694.
25. Bender, C. J., Sahlin, M., Babcock, G. T., Barry, B. A., Chandrashekar, T. K., Salowe, S. P., Stubbe, J., Lindström, B., Petersson, L., Ehrenberg, A., and Sjöberg, B.-M. (1989) An ENDOR study of the tyrosyl free radical in ribonucleotide reductase from *Escherichia coli*. *J. Am. Chem. Soc. 111*, 8076–8083.
26. Gilchrist, M. L., Jr., Ball, J. A., Randall, D. W., and Britt, R. D. (1995) Proximity of the manganese cluster of photosystem II to the redox-active tyrosine Y_Z. *Proc. Natl. Acad. Sci. U.S.A. 92*, 9545–9549.
27. Whittaker, M. M., and Whittaker, J. W. (2000) Expression of recombinant galactose oxidase by *Pichia pastoris*. *Protein Expression Purif. 20*, 105–111.
28. Whittaker, M. M., and Whittaker, J. W. (2005) Construction and characterization of *Pichia pastoris* strains for labeling aromatic amino acids in recombinant proteins. *Protein Expression Purif. 41*, 266–274.
29. Griffiths, D. V., Feeney, J., Roberts, G. C. K., and Burgen, A. S. V. (1976) Preparation of selectively deuterated aromatic amino acids for use in ^{1}H NMR studies of proteins. *Biochim. Biophys. Acta 446*, 479–485.
30. Olsen, J. C. (1905) *A Textbook of Quantitative Chemical Analysis*, 2nd ed., revised, pp 165−168, D. Van Nostrand, New York.
31. Poole, C. P., Jr. (1983) *Electron paramagnetic resonance. A comprehensive treatise on experimental techniques*, 2nd ed., p 443, John Wiley, New York.
32. Cregg, J. M. (2007) *Pichia Protocols*, 2nd ed., Humana Press, Totowa, NJ.
33. Whittaker, M. M., and Whittaker, J. W. (1988) The active site of galactose oxidase. *J. Biol. Chem. 263*, 6074–6080.
34. Hales, B. J. (1993) Intrinsic and extrinsic paramagnets as probes of metal clusters. *Methods Enzymol. 227*, 384–395.
35. Griffin, M., Muys, A., Noble, C., Wang, D., Eldershaw, C., Gates, K. E., Burrage, K., and Hanson, G. R. (1999) XSophe, a computer simulation software suite for the analysis of electron paramagnetic resonance spectra. *Mol. Phys. Rep. 26*, 60–84.
36. Engström, M., Himo, F., and Ågren, H. (2000) Ab initio g-value calculations of the thioether substituted free radical in galactose oxidase. *Chem. Phys. Lett. 319*, 191–196.
37. Atherton, N. M. (1993) *Principles of Electron Spin Resonance*, Ellis Horwood, New York.
38. Adamo, C., Barone, V., and Subra, R. (2000) The mechanism of spin polarization in aromatic free radicals. *Theor. Chem. Acc. 104*, 207–209.
39. Heller, H., and McConnell, H. (1960) Radiation damage in organic crystals. II. ESR of $(CO_2H)CH_2CH(CO_2H)$ in 3-succinic acid. *J. Chem. Phys. 32*, 1535–1539.
40. Svistunenko, D. A., and Cooper, C. E. (2004) A new method for identifying the site of tyrosyl radicals in proteins. *Biophys. J. 87*, 582–595.
41. McConnell, H. M. (1956) Electron densities in semiquinones by paramagnetic resonance. *J. Chem. Phys. 24*, 632.
42. Morton, J. R., and Preston, K. F. (1978) Atomic parameters for paramagnetic resonance data. *J. Magn. Reson. 30*, 577–582.
43. Karplus, M., and Fraenkel, G. K. (1961) Theoretical interpretation of carbon-13 hyperfine interactions in electron spin resonance spectra. *J. Chem. Phys. 35*, 1312–1323.
44. Broze, M., and Luz, Z. (1969) Semiempirical and theoretical derivation of oxygen-17 σ-π interaction constants in carbonyl-containing anion radicals. *J. Chem. Phys. 51*, 738–753.
45. Bramwell, F. B., Haddon, R. C., Wudl, F., Kaplan, M. L., and Marshall, J. H. (1978) Electron spin resonance studies of sulfur-based donor heterocycles: sulfur-33 couplings. *J. Am. Chem. Soc. 100*, 4612–4614.
46. Sullivan, P. D. (1968) Hyperfine splittings from naturally occurring sulfur-33 in electron paramagnetic resonance spectra. *J. Am. Chem. Soc. 90*, 3618–3622.
47. Miura, Y., Isogai, M., and Kinoshita, M. (1983) Triphenylmethyl-substituted arylthioaminyl radicals. An ESR study of N-(arylthio)triphenylmethylaminyls. *Chem. Soc. Jpn. 58*, 751–752.
48. Bonozzola, L., Fackir, L., Leray, N., and Roncin, J. (1984) ESR study of some sulfur-centered radicals formed in irradiated cysteamine and 1,4-dithiane single crystals. *Radiat. Res. 97*, 462–467.
49. Hadley, J. H., Jr., and Gordy, W. (1975) Nuclear coupling of ^{33}S and the nature of free radicals in irradiated crystals of cysteine hydrochloride and N-acetyl methionine. *Proc. Natl. Acad. Sci. U.S.A. 72*, 3486–3490.
50. Amorati, R., Catarzi, F., Menichetti, S., Pedulli, G. F., and Viglianisi, C. (2008) Effect of *ortho*-SR groups on O-H bond strengths and H-atom donating ability of phenols: A possible role for the Tyr-Cys link in galactose oxidase active site? *J. Am. Chem. Soc. 130*, 237–244.

BI800305D